Cascaded Graph Convolution Approach for Nuclei Detection in Histopathology Images

Sachin S. Bahade*, Michael Edwards, and Xianghua Xie

Department of Computer Science, Swansea University, UK; Email: {michael.edwards, x.xie}@swansea.ac.uk
*Correspondence: s.s.bahade.885875@swansea.ac.uk (S.S.B.)

***Abstract*—Nuclei detection in histopathology images of cancerous tissue stained with conventional hematoxylin and eosin stain is a challenging task due to the complexity and diversity of cell data. Deep learning techniques have produced encouraging results in the field of nuclei detection, where the main emphasis is on classification and regression-based methods. Recent research has demonstrated that regression-based techniques outperform classification. In this paper, we propose a classification model based on graph convolutions to classify nuclei, and similar models to detect nuclei using cascaded architecture. With nearly 29,000 annotated nuclei in a large dataset of cancer histology images, we evaluated the Convolutional Neural Network (CNN) and Graph Convolutional Networks (GCN) based approaches. Our findings demonstrate that graph convolutions perform better with a cascaded GCN architecture and are more stable than centre-of-pixel approach. We have compared our two-fold evaluation quantitative results with CNN-based models such as Spatial Constrained Convolutional Neural Network (SC-CNN) and Centre-of-Pixel Convolutional Neural Network (CP-CNN). We used two different loss functions, binary cross-entropy and focal loss function, and also investigated the behaviour of CP-CNN and GCN models to observe the effectiveness of CNN and GCN operators. The compared quantitative F1 score of cascaded-GCN shows an improvement of 6% compared to state-of-the-art methods.**

***Keywords*—Nuclei detection, graph convolution network, medical imaging**

I. Introduction

Nuclei detection in histology images is an important parameter for many biomedical image analysis tasks. Due to the varying sizes and shapes of the nuclei, detecting accurate nuclei becomes a challenging task. In the past, many methods have been proposed, which can be categorised into classification and regression approaches. Since graph convolution networks are becoming more popular, solving this hard task in an irregular domain is important because it gives graph convolution the power and possibility to work on critical data.

The tumour is the result of the cell's utterly unrestrained development and demise. In the formation of tumours, this cell heterogeneity causes inflammation, angiogenesis, and tumour necrosis [1, 2]. The location, size, configuration, and placement of these diverse cell types also, reveal the many cancer-related stages [3, 4]. Therefore, the qualitative and quantitative analysis of nuclei helps to understand the condition of the tumour better and explore the different options for various cancer treatments. Pathologists use different colour markers and stains to understand many properties of cancer tissues. However, to identify informative markers, biological experts must have a thorough understanding of tumours, and also it is costly to repeatedly perform lab work and have access to cell data, which is not always available [5]. Creating an automated system to find nuclei would be a better way to save time in the lab while also allowing for effective analysis that would help biological professionals understand the different conditions of the tissue cell.

There are many factors that affect the precise automation of the nuclei detection, mainly the noise and poor staining during the preparation process of the image slides. Disarrangement of nuclei, diversity of nuclear morphology, and complex tissue structure create a challenging task for computer vision researchers to automate and analyse. In addition, different types of cells often have irregular chromatin textures and seem to largely overlap each other, having a fairly visible boundary, which makes the detection of individual nuclei a challenging task. One more thing that makes it hard to automate the process of detecting nuclei is that there are so many different types of nuclei that look like the same type of nuclei [6].

However, many cell detection methods have been developed based on classification, regression, and conventional methods such as thresholding, region-growing, K-means, and so on. Sirinukunwattana *et al.* [6] proposed a regression-based approach to train a convolutional neural network model to predict the centre coordinate of the nuclei used in the probability map carried by post-processing. In this method, the spatially constrained layer is used for regression-based nuclei centre coordinate prediction, and the parameter estimation layer is used to create a probability map. This work is influenced by the conventional method for object detection as centre-of-the-pixel CNN (CP-CNN), where each path gives the probability of being the centre of nuclei or not, and second, work structural regression (SR-CNN) [7] where each patch is regressed instead of a single pixel. Veta *et al.* [8] proposed techniques for nucleus detection in routine H&E histology images that rely on morphological features such as symmetry and stability of the nuclear region to identify

Manuscript received July 12, 2022; revised September 22, 2022; accepted October 23, 2022.

nuclei, and the direction of the gradient tells where the centre of nucleus is. Cosatto *et al.* [9] use the Difference of Gaussian (DoG) and Hough transform to find symmetric shapes of cells for nuclei detection.

There are many other methods that use the classification approach for cell detection. In images of breast cancer that have been stained with H & E, morphological features are one of the foundations for how cancer, lymphocytes, and stromal cells are classified. To do this, nuclei need to be segmented [10]. Lekha S Nair *et al.* [11] propose an immediate single-step detection approach with the use of the YOLOv4 model for mitotic nuclei detection in breast histopathology images where the model is trained to carry out classification and bounding box regression at a similar time. Malon *et al.* [12] used a CNN classifier for mitotic and non-mitotic cell classification using colour, texture, and shape information, and Nguyen *et al.* [13] also classified nuclei based on their texture and appearance. Cruz *et al.* [14] showed that deep learning approaches produce superior results compared to a predefined bag of features and canonical representation. In some of the recent work, Chenchen *et al.* [15] proposed a complex semi-supervised learning framework, which optimises the detection network with the involvement of unlabeled image reconstruction. Whereas Wang *et al.* [16] proposed a cascaded classifier to detect mitotic cells. Alom *et al.* [17] proposed systems that use three different deep learning models for nuclei classification, segmentation, and detection tasks. We suggested a cascading strategy for nuclei detection in histopathology images, drawing inspiration from the architectures employed in study [6] and recent advances in the graph convolution irregular data generalisation approach.

In the second section that follows, we go through how graph convolution works and how to construct a cascaded architecture for detection. The dataset used and experiment findings are then explored in Section III, which is followed by Section IV of Conclusion.

II. Methods

The problem of nuclei detection consists of finding a set of centroid coordinates of nuclei from a given input RGB image *I*. This problem is solved by a graph convolution-based deep learning supervised approach where the detector is trained on training samples with ground truth information about centroid coordinates. Each pixel is categorised into nuclei or non-nuclei classes. Our detector is a GCN-based pixel classifier. All pixels in each training sample are assigned to one of two classes: nuclei, in which the ground-truth pixel p is centred on the training sample, and non-nuclei, in which the centred pixel is not within Euclidean distance d of ground-truth nuclei. The GCN network predicts that the class of the raw RGB image value will fall into the sample patch.

A. Detecting Nuclei with GCN

The architecture of the network is shown in Fig. 1. It consists of two graph convolution networks followed by two fully connected layers. The RGB pixel values of each sample are passed through the graph convolution operator to extract the features. The extracted feature vector is classified by fully connected layers. The last layer is a single unit dense classification layer with sigmoid non-linearity. There are dropout and ReLU non-linear activation functions that are used before each dense layer to keep it from overfitting.

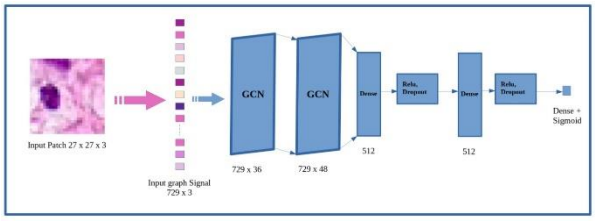

Figure 1. Graph convolution architecture.

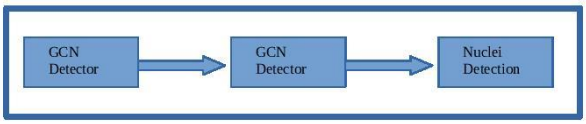

Figure 2. Cascade GCN pipeline. Left to right – Stage 1, Stage 2, detection with NMS.

We formulate nuclei detection as a simple binary classification problem. The architecture of the method is depicted in Fig. 1. Given an input histology image of size 500×500, it extracts patches of size 27×27 with centre coordinates as ground truth nuclei centre as positive samples. To extract negative samples, we have chosen random coordinates which do not fall into the proximity of the ground truth nuclei centre *c* with distance *d* as shown below,

$$Sample = \begin{cases} Positive, & \forall c, \\ Negative, & dist(Nc - c) > d, \end{cases}$$

where Nc is the random nuclei centre.

To formulate the classification, we have labelled positive patches as 1 and negative patches as 0. The number of negative samples that must be extracted from each image has been randomly determined. We have used the spectral-based graph convolutional operator to learn features. To perform graph convolution, the patch of size 27×27 is considered as a 2D grid graph having a set of nodes (V), a set of weighted edges (E), and a binary adjacency matrix (A) of size 729×729 with the property that each node is connected with its neighbouring nodes, which form the basis of locality for the convolution operation.

The graph structure of the image represents 2D grids of regular data and graph Laplacian is the core operator for the graph convolution layer. One form of the Laplacian operation is represented as $L = D - A$, where D is the degree matrix and A, is the adjacency matrix. The Normalized Laplacian matrix is $L = I_n - D^{-1/2}AD^{-1/2}$ where I_n is the identity matrix that considers self-node features. The Laplacian matrix is decomposed into orthonormal vectors $U = u_{i=1\ldots N}$ where u_i is an eigenvector associated with eigenvalues $\lambda_{i=1\ldots N}$. Apply graph Laplacian and then eigendecomposition of the graph

Laplacian matrix, which gives the Fourier modes and graph frequencies [18]. In graph signal processing, a graph signal s is a feature vector that lies on the node of the graph. When the graph Fourier transform (F_G) is applied to signal s using a matrix U, the result is,

$$F_G(s) = \hat{s} = U^T s \tag{1}$$

Then the inverse graph Fourier transform is applied which gives original signal s [18, 19],

$$F^{-1}(\hat{s}) = U\hat{s} = UU^T s = s, \tag{2}$$

Now the convolution of signal s with a filter g in Fourier domain is defined as,

$$s \underset{G}{*} g = F_G^{-1}(F_G(s) \odot g), \tag{3}$$

and can be represented in,

$$s \underset{G}{*} g = \hat{g}(L)s, \tag{4}$$

After the graph convolution layer, there are two fully connected layers, with the last layer having one neuron activated by a sigmoid function to classify the feature vector extracted from the previous two graph convolutional layers. This graph convolutional layer-based classifier is used in a cascaded architecture to improve nuclei detection while maintaining a high recall value.

B. Cascaded GCN

The cascade method progressively removes negative samples at each stage. As an adverse reaction to the filtering process, some of the positive samples were also eliminated. Fig. 1 architecture used for classification filtering, and Fig. 2 shows the complete flowchart of the Cascade GCN detector. It consists of two phases. soft negative and hard negative elimination. Classification patches are generated by scanning input images in a sliding window fashion, with height and width shifting by one pixel. A large number of window patches were eliminated as background in the first stage. Among the positive samples remaining from the first stage, a false positive sample is further eliminated by the hard negative elimination of the second stage. The final detection is achieved by passing the remaining samples through Non-Maximum Suppression (NMS) [20].

In the soft negative elimination first stage of the cascaded-GCN, a large number of patches are generated by the sliding window method with window shifting one pixel at a time to save any loss of features in the image for training. Fig. 1 provides the architecture used for first-stage soft negative patch removal where two graph convolutional network layers and two fully connected layers are used. Utilizing such an architecture is inspired by the previous CNN-based architecture for nuclei detection in CP-CNN and SP-CNN. In this architecture, the input 2D grid graph 27×27 has a binary adjacency matrix of size 729×729 and the input graph signal has been normalised between 0 and 1 by the normalisation function,

$$X = \left(\frac{X - \mu}{\sigma}\right) \tag{5}$$

where X = image data, μ = mean and σ = standard deviation. Each node in the graph holds a three-channel RGB signal. The number of filters used in the first and second GCN is 36 and 48, which helps to preserve the desirable features and remove low-frequency features. To retain the most positive patches for the following stages, a high recall is achieved by training over the maximum precision-recall rate for patience level 10 and using a sigmoid classification layer with a decision boundary of 0.50 for evaluation. For example, the two-fold cross-validation recall rate for evaluation is 84.53%, but this higher value comes at the cost of a lowered precision rate of 65.45%.

The filtered positive samples from stage 1 are passed to stage 2, which is the hard negative elimination stage, where positive patches obtained from the previous stage are taken into consideration for the training stage 2 model. With the help of ground truth, the positive sample was separated into true positive and false positive. Here, if the predicted nucleus centre is close enough to the ground truth nucleus centre with a pixel distance less than d, it is considered a true positive and a false positive the other way around.

To maintain high recall in stage 1 and remove hard negative samples, another model with the same architecture as in Fig. 1 is used and trained for minimum validation loss with patience 10. In our case, 38,643 false-positive and 100,000 true-positive samples are used for training in the second stage. To balance the data for training, negative samples are added by flipping them right and rotating them 90 degrees.

The nuclei detection block is designed to accurately locate the nuclei location by retaining efficient positive patch samples at higher resolution. Nuclei detection is the last phase of the cascade pipeline. Binary classification is carried out in the last two phases, filtering most negative samples while maintaining higher precision and recall. With an intersection over union threshold of 0.30 and a maximum output bounding box size of 1200, the remaining positive samples with nuclei in the same place were put through a non-maximum suppression to get rid of duplicates.

III. Experiment and Results

A. Dataset and Implementation

The dataset used consists of 100 H&E stained histology images of adenocarcinoma. This dataset is used for the CNN-based nucleus detection problem. Each image has a size of 500×500 pixels. These images contain some noise, for example, over-staining and failed autofocus. Annotation of the nuclei is marked by the experts, and there are 29756 nuclei centred for detection purposes in supervised learning. These slide images of size 500×500 are used for the extraction of patches of size 27×27 for training and validation data for models. Fig. 3 shows the

original image and extracted patches, each patched with a green colour box. Patches are extracted randomly where coordinates fall within a proximity radius $d \leq 2$ categorised as a positive sample and negative elsewhere.

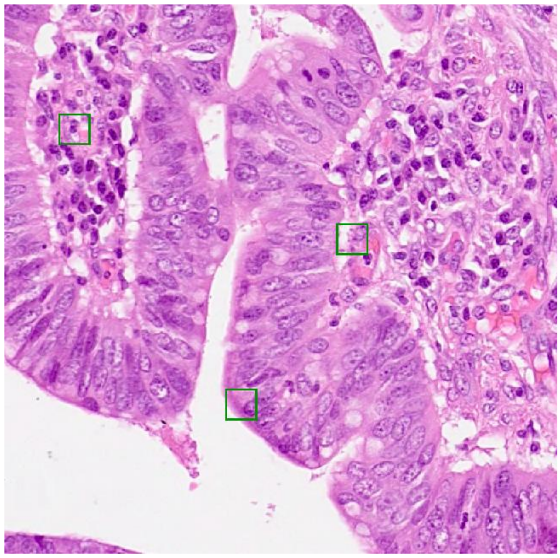

(a) H & E image of size 500×500

(b) Patch 1 (c) Patch 2 (d) Patch 3

Figure 3. Data Extraction. 3a, shows the original images of size 500×500 obtained from the slides. Whereas 3b, 3c, 3d refers to extracted patched of size 27×27.

Our model is implemented in Tensorflow 2.0 and Keras. The proposed model is trained and evaluated on a PC with an Intel i7 CPU and an NVIDIA GEFORCE GTX 1080Ti. For a fair comparison, the learning rate is set at 0.001 and the batch size is 100, and a dropout rate of 0.2 is used for CP-CNN and the proposed model GCN. We have also tested both with binary cross-entropy and focal loss to see the behaviour of both models in different loss environments. For SC-CNN implementation, we have set the learning rate at 0.01 and scheduled learning as suggested by Sirinukunwattana *et al.* [6].

B. Model Evaluation

Fig. 4 shows the qualitative detection results on the unseen sample images. For quantitative analysis, we define the ground-truth areas as blue circular regions with 8 pixels around every annotated nuclei centre. A detected nuclear centroid is considered a true positive (TP) only if it lies within the ground-truth areas; otherwise, it is considered a false positive (FP). Each TP is matched with the nearest ground-truth annotated nuclei centre. The ground-truth nuclei centres that are not matched by any detected results are considered false negatives (FN). We can calculate the precision*(P)*, recall*(R)*, and F_1 score using the above definitions: $P = \frac{TP}{TP+FP}$, $R = \frac{TP}{TP+FN}$ and $F_1 = \frac{2PR}{P+R}$ respectively.

We evaluated the proposed model with *CNN-based Pixel-Wise Classification* (PWC) [7] , or *Centre of Patch Convolutional Neural Network* (CP-CNN) [6] which shares the same architecture as mentioned in the paper [6] except that it utilises the sigmoid activation in the last layer and no graph.

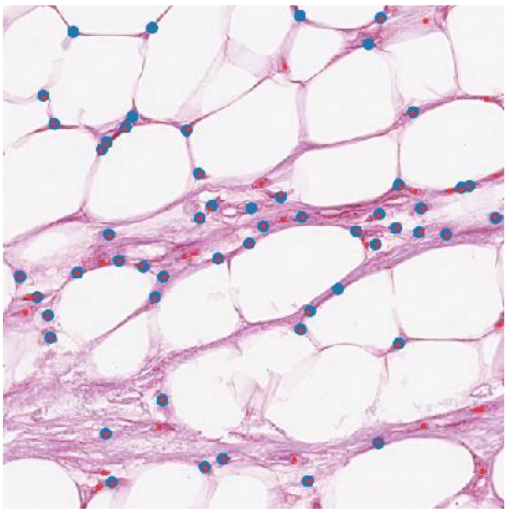

(a). SC-CNN

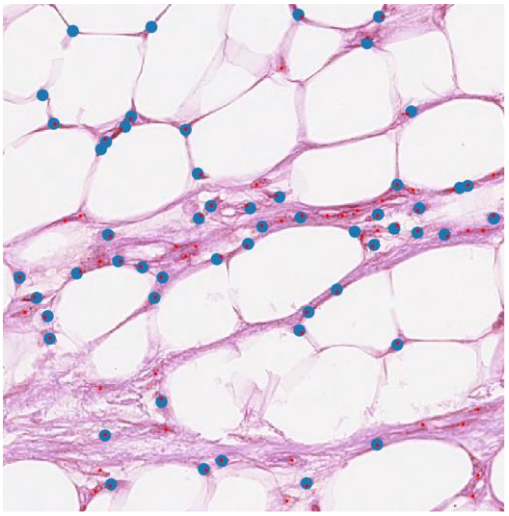

(b). CP-CNN

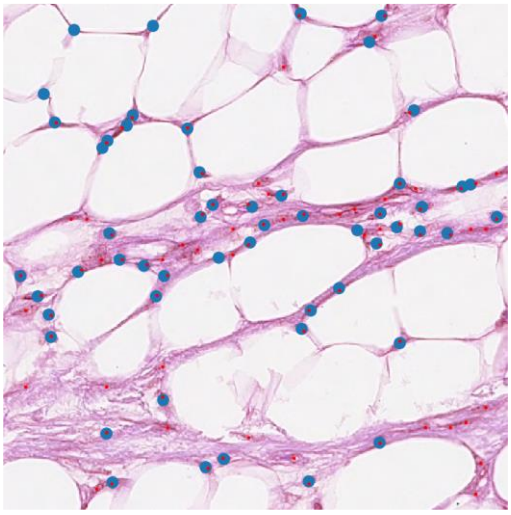

(c). GCN

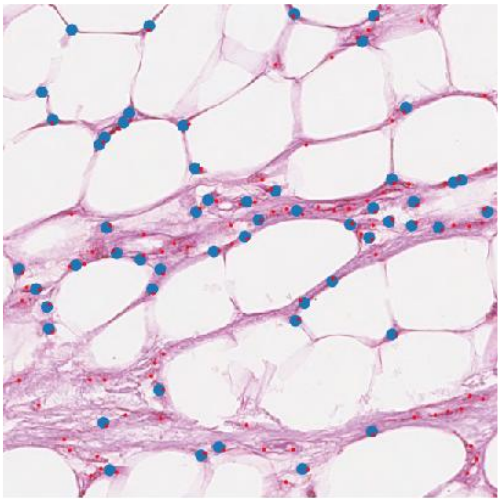

(d). Cascade-GCN

Figure 4. Nuclei detection results on the sample image. Red dots represent the detected nuclei centre. The ground-truth annotations are represented by blue circles for better illustrations.

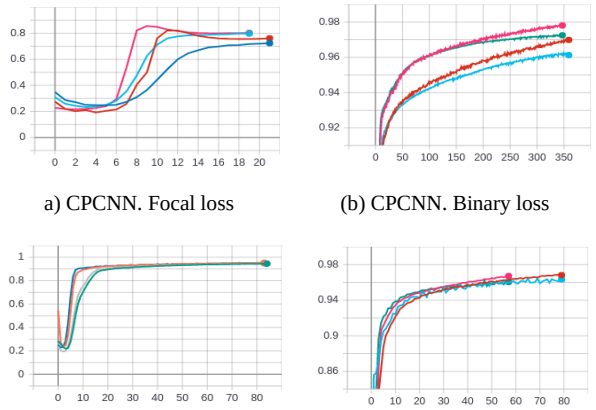

a) CPCNN. Focal loss

(b) CPCNN. Binary loss

(c) GCN. Focal loss

(d) GCN. Binary loss

Figure 5. Qualitative Comparison of Results. The figure shows the 2-fold training/validation curves. 4a. bluetr1, redva1, skytr2, pinkva2, 4b. redtr1, skyva1, pinktr2, greenva2, 4c. greentr1, grayva1, Orangetr2, blueva2, 4d. redtr1, skyva1, pinktr2, greenva2.

TABLE I. QUANTITATIVE RESULTS

Method	Precision	Recall	F1
SC-CNN (lr 0.01)	0.7183 ± 0.0063	0.6995 ± 0.0579	0.7078 ± 0.0328
SC-CNN (lr scheduled)	0.6355 ± 0.1163	0.7909 ± 0.0416	0.6951 ± 0.0555
CP-CNN (Bin cross)	0.7291 ± 0.0677	0.6930 ± 0.0227	0.7078 ± 0.0203
CP-CNN (Focal Loss)	0.0 ± 0.0	0.0 ± 0.0	0.0 ± 0.0
GCN (Bin cross)	0.6832 ± 0.0019	0.6757 ± 0.0141	0.6793 ± 0.0061
GCN (Focal Loss)	**0.7336** ± 0.0055	0.6077 ± 0.0028	0.6647 ± **0.0005**
Cascade-GCN (Focal Loss)	**0.7334** ± **0.0004**	**0.7927** ± **0.0005**	**0.7619** ± **0.0005**

Fig. 5 shows the validation precision-recall curves with respect to the epochs of the GCN method and CP-CNN. These curves are generated over the maximum precision-recall metric with patience 10. Fig. 4b demonstrates that the CP-CNN is unable to learn features over the focal loss, and their quantitative evaluation results are explained in Table I. While using the binary cross-entropy loss for CP-CNN, there is a large deviation between the two folds as compared to the proposed model using GCN. The GCN-based model can learn features better in focal loss, but it also works for binary cross-entropy loss, which is not true in the case of CP-CNN focal loss. Also, the deviation between the folds in the case of GCN is smaller compared to CP-CNN, which shows the stability of the GCN-based proposed model.

C. Comparison with Other Works

We also compared our model with the state-of-the-art proximity map-based nuclei detection regression model (SC-CNN) [13]. While comparing with SC-CNN, we have eliminated the preprocessing of augmentation and HSV space channel separation to keep training data the same for all methods for comparison. As shown in Table I, there is a huge difference between precision and recall value for SC-CNN with a stable learning rate and a scheduled learning rate. With careful observation of standard deviation values, we can see that the GCN-based proposed model performs better in precision, recall, and F1 score. While compared with the SC-CNN scheduled learning rate, the GCN precision value has increased by almost 10%. One of the advantages of our GCN model with focal loss, it learns features better while CP-CNN struggles to learn hardly any features, which proves the stability of the GCN-based model. The value 0.0 ± 0.0 in Table I explains the testing results of the CP-CNN (Focal Loss) model's learning ability over the focal loss function compared to binary cross-entropy loss. As shown in Table I, when using the GCN in a cascade fashion, the F1 score increases by almost 6%. While observing the Cascade qualitative results in Fig. 4d, it has a higher recall value than the others but at the expense of a lower precision, whereas two-fold quantitative evaluation results on 50 images in Table I, show overall precision, recall, and F1 score are higher.

IV. CONCLUSION

In this paper, we propose a cascaded graph convolution approach for the nuclei detection task. The proposed GCN classifier differs from the traditional CNN classifier by introducing a graph convolutional operator to learn features in the training data. We have experimentally demonstrated the superior performance of the cascaded architecture of the GCN classifier in terms of the stability and precision, recall, and F1 score compared with the CNN-based state-of-the-art and observed the validation behaviour of CPCNN and GCN with different loss functions. In the future, we hope to improve the performance by adding more classifiers and using other graph convolutional operators.

CONFLICT OF INTEREST

The authors declare no conflict of interest.

AUTHOR CONTRIBUTIONS

Sachin S. Bahade conducted the research and wrote with support from Michael Edwards and Xianghua Xie supervised the project and provided suggestions and recommendations along the way. All authors had approved the final version.

REFERENCES

[1] P. P. Dalerba, T. Kalisky, D. Sahoo, *et al.*, "Single-cell dissection of transcriptional heterogeneity in human colon tumors," *Nature Biotechnology*, vol. 29, no. 12, pp. 1120–1127, 2011.

[2] C. A. O'Brien, *et al.* "A human colon cancer cell capable of initiating tumour growth in immunodeficient mice," *Nature*, vol. 445, no. 7123, pp. 106–110, 2007.

[3] A. Basavanhally, A. Pollett, S. Gallinger, *et al.*, "Multi-field-of-view strategy for image-based outcome prediction of multi-parametric estrogen receptor-positive breast cancer histopathology: Comparison to Oncotype DX," *Journal of Pathology Informatics*, vol. 2, 2011.

[4] J. S. Lewis Jr, S. Ali, J. Luo, *et al.*, "A quantitative histomorphometric classifier (QuHbIC) identifies aggressive versus indolent p16-positive oropharyngeal squamous cell carcinoma," *The American Journal of Surgical Pathology*, vol. 38, no. 1, p. 128, 2014.

[5] G. N. P. V. Muijen, D. J. Ruiter, W. W. Franke, *et al.*, "Cell type heterogeneity of cytokeratin expression in complex epithelia and carcinomas as demonstrated by monoclonal antibodies specific for cytokeratins nos. 4 and 13," *Experimental Cell Research*, vol. 162, no. 1, pp. 97–113, 1986.

[6] K. Sirinukunwattana, S. E. Raza, Y. W. Tsang, *et al.*, "Locality sensitive deep learning for detection and classification of nuclei in routine colon cancer histology images," *IEEE Transactions on Medical Imaging*, vol. 35, no. 5, pp. 1196–1206, 2016.

[7] Y. Xie, F. Xing, X. Kong, *et al.*, "Beyond classification: Structured regression for robust cell detection using convolutional neural network," in *Proc. International Conference on Medical Image Computing and Computer-Assisted Intervention*, 2015, pp. 358–365.

[8] M. Veta, J. P. W. Pluim, P. J. V. Diest, *et al.*, "Breast cancer histopathology image analysis: A review," *IEEE Transactions on Biomedical Engineering*, vol. 61, no. 5, pp. 1400–1411, 2014.

[9] E. Cosatto, M. Miller, H. P. Graf, *et al.*, "Grading nuclear pleomorphism on histological micrographs," in *Proc. International Conference on Pattern Recognition*, 2008, pp. 1–4.

[10] Y. Yuan, H. Failmezger, O. M. Rueda, *et al.*, "Quantitative image analysis of cellular heterogeneity in breast tumors complements genomic profiling," *Science Translational Medicine*, vol. 4, no. 157, 2012.

[11] L S Nair, R. Prabhu, G. Sugathan, *et al.*, "Mitotic nuclei detection in breast histopathology images using YOLOv4," in *Proc. 12th International Conference on Computing Communication and Networking Technologies (ICCCNT)*, 2021, pp. 1–5. DOI: 10.1109/ICCCNT51525.2021.9579969

[12] C. D. Malon and E. Cosatto, "Classification of mitotic figures with convolutional neural networks and seeded blob features," *Journal of Pathology Informatics*, vol. 4, 2013.

[13] K. Nguyen, A. K. Jain, and B. Sabata. "Prostate cancer detection: Fusion of cytological and textural features," *Journal of Pathology Informatics*, vol. 2, 2011.

[14] A. A. Cruz-Roa, J. E. A. Ovalle, A. Madabhushi, *et al.*, "A deep learning architecture for image representation, visual interpretability and automated basal-cell carcinoma cancer detection," in *Proc. International Conference on Medical Image Computing and Computer-Assisted Intervention*, 2013, pp. 403–410.

[15] C. Tian, L. Su, Z. Wang, *et al.*, "Semi-supervised nuclei detection in histopathology images via location-aware adversarial image reconstruction," *IEEE Access*, vol. 10, pp. 42739–42749, 2022. DOI: 10.1109/ACCESS.2022.3168721

[16] H. Wang, A. Cruz-Roa, A. Basavanhally, *et al.*, "Cascaded ensemble of convolutional neural networks and handcrafted features for mitosis detection," *Medical Imaging, Digital Pathology, International Society for Optics and Photonics*, vol. 9041, 2014.

[17] Z Alom, V. K. Asari, A. Parwani, *et al.*, "Microscopic nuclei classification, segmentation, and detection with improved deep convolutional neural networks (DCNN)," *Diagnostic Pathology*, vol. 17, no. 1, pp. 1–17, 2022.

[18] M. Defferrard, X. Bresson, and P. Vandergheynst, "Convolutional neural networks on graphs with fast localized spectral filtering," *Advances in Neural Information Processing Systems*, pp. 3844–3852, 2016.

[19] S. Bahade, M. Edwards, and X. Xie, "Graph convolution networks for cell segmentation," in *Proc. International Conference on Pattern Recognition Applications and Methods*, 2021, pp. 620–627.

[20] N. Bodla, B. Singh, R. Chellappa, *et al.*, "Soft-NMS–improving object detection with one line of code," in *Proc. the IEEE International Conference on Computer Vision*, 2017, pp. 5561–5569.

Sachin S. Bahade received his B.Eng. degree in information technology from Amaravati University, India in 2009 and the M.Tech. in computer science and engineering from Nagpur University, India in 2014. He is currently a PhD student at Swansea University, United Kingdom. His research focus on Irregular domain deep learning, segmentation, and detection in medical imaging.

Michael Edwards received his MSc (2013) and PhD (2018) degrees in the field of computer SCIence from Swansea University (UK), and currently holds a post of lecturer within the Computer Science Department. His main research interests are broadly in the areas of machine learning and image processing, with particular focus on representation learning on graphs, deep learning on irregular domains, and human-in-the-loop AI. His main applications are in topics of human action recognition, medical imaging, and place retrieval.

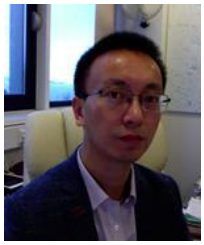

Xianghua Xie (Senior Member, IEEE) received the M.Sc. and Ph.D. degrees in computer science from the University of Bristol, Bristol, U.K., in 2002 and 2006, respectively. He is currently a Professor with the Department of Computer Science, Swansea University, Swansea, U.K., where he is leading the Computer Vision and Machine Learning Laboratory, Swansea University. He has published more than 170 refereed conference and journal publications and (co-)edited several conference proceedings. His research interests include various aspects of pattern recognition and machine intelligence and their applications to real-world problems. Dr. Xie is an executive member of British Machine Vision Association (BMVA). He is an Associate Editor of a number of journals, including Pattern Recognition and IET Computer Vision.